

In Silico Studies of Active Probe Dynamics in Crowded Media

Ligesh Theeyancheri, Rajiblochan Sahoo, Praveen Kumar, and Rajarshi Chakrabarti*

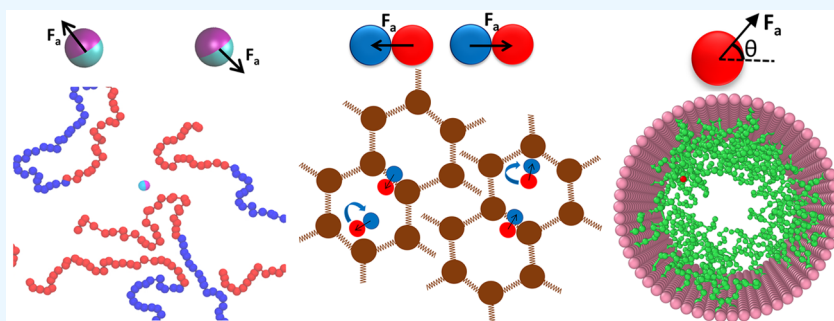
Cite This: *ACS Omega* 2022, 7, 33637–33650

Read Online

ACCESS |

Metrics & More

Article Recommendations



ABSTRACT: Active systems are made of agents, each of which takes energy from the environment and converts it to directed motion. Therefore, by construction, these systems function out of equilibrium and cannot be described using equilibrium statistical mechanics. Though the most studied aspect has been the collective motion of active particles, the motion at the individual particle level in crowded media is also of prime importance. Examples include the motion of bacteria in hydrogels, single cell migration as a way to search for food or escape from toxic agents, and synthetic active agents transporting through soft crowded media. This review presents an overview of our understanding of single active probe dynamics in crowded media from computer simulations. The active probe is a Janus or a dumbbell-shaped particle, and the medium is made of crowders that are either sticky or repulsive to the probe and could be frozen or mobile. The density and the topology of the crowders also play an important role. We hope our in silico studies will help to elucidate the mechanism of activity-driven transport in crowded media in general and design nanomachines for targeted delivery.

1. INTRODUCTION

Active matter refers to a system, made of constituents, each of which is driven out of equilibrium by consuming energy from the environment and converting it to a directed motion.¹ Molecular machines like kinesin or myosin motor proteins inside biological cells trigger the movement or transport of biomolecules and lead to the intrinsic out-of-equilibrium state of these systems.² The nature of these living and active matter systems implies broken detailed balance, nonthermal fluctuations, and violation of the fluctuation–dissipation relation, which makes their theoretical description particularly a challenging task.¹ They feature many novel behaviors such as the activity-driven phase separation³ or large-scale collective motion⁴ that are not achievable by systems at equilibrium, and their properties can be explained and understood only within the framework of non-equilibrium physics. In biological systems, force generation by ATP hydrolysis and directed motion of cells are essential in cellular processes, including cell motility, cell multiplication, and intracellular transport.² The processes such as oscillations of the mitotic spindle during asymmetric cell division,⁵ microbial pathogens in stomach mucus, periodic flagellar beating for locomotion, or motility of spermatozoa by ciliary beating through cervical mucus are the

paradigmatic examples of non-equilibrium events occurring in the biological realm. In recent years, researchers made significant and growing efforts to uncover the underlying physics and explore their applications in diverse fields. This leads to the development of novel strategies for designing artificial microswimmers and nanoswimmers like Janus particles,^{6,7} chiral particles, and catalytic nanomotors¹⁶ that are capable of self-propulsion to mimic their biological counterparts.

In general, the motion of passive particles is governed by equilibrium thermal fluctuations owing to random collisions with the surrounding fluid molecules,⁸ while the active particles are driven by the interplay between random fluctuations and self-propulsion that drives them out of equilibrium.¹ To describe the motion of active particles, researchers have proposed different models, such as active

Received: July 26, 2022

Accepted: September 7, 2022

Published: September 15, 2022



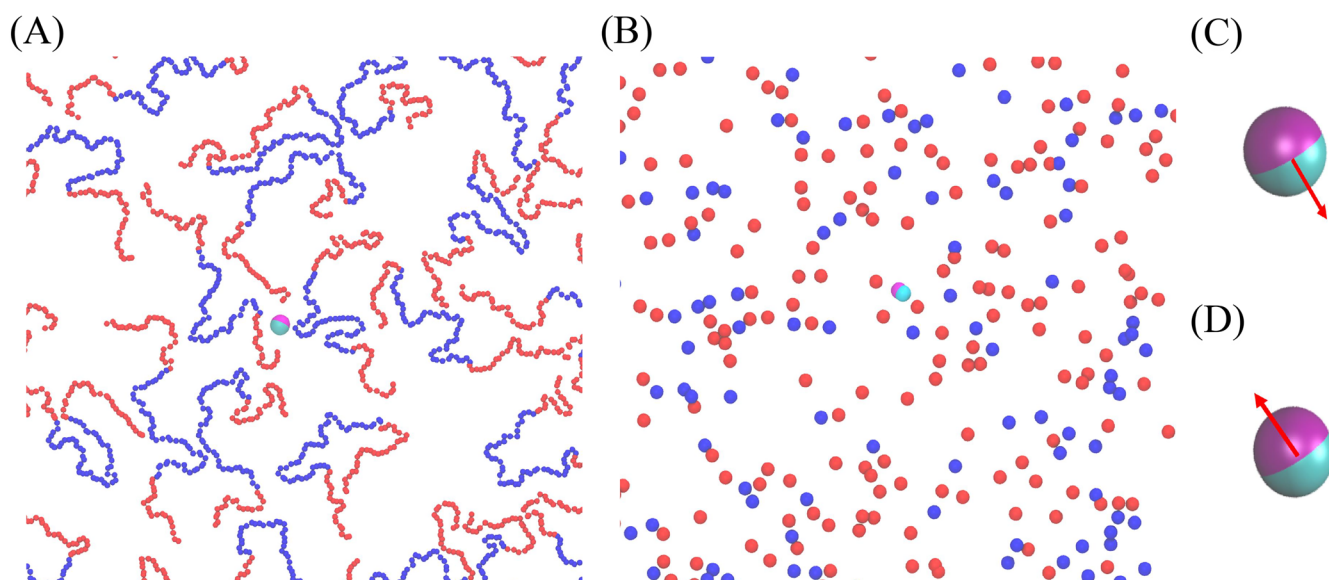


Figure 1. Snapshot of a self-propelled Janus probe in (A) polymers with sticky zones and (B) binary mixture of colloids with sticky and nonsticky interactions (in both cases, the magenta part of the Janus probe has an attractive interaction with blue colored beads). A schematic illustration of the direction of self-propulsion toward the (C) nonsticky face and (D) sticky face of the self-propelled Janus probe. Reproduced and customized with permission from ref 9. Copyright 2020 Royal Society of Chemistry.

Brownian particles,^{1,9} active Ornstein–Uhlenbeck particles,^{10,11} and run and tumble particles.¹ The dynamics of active Brownian particles become the central focus of the physical and biophysical research communities. In the last few decades, several studies are reported, which try to reveal the physics behind the novel features exhibited by the active Brownian particles in complex media.^{9,11–14} However, the real-life situations are quite different, and hence there is a growing interest in understanding the dynamics of these active Brownian particles in complex environments such as porous soils, sediments, and living tissues. There are multiple factors like crowding and local heterogeneity that either enhance or limit the diffusion of active agents moving through these complex media for performing their assigned tasks.

In this review, we provide a guided tour through our previous attempts to understand the physics underlying the motion of active agents in crowded environments. In free space, the active probe particles freely diffuse in the available space,¹ whereas the same active probe behaves differently in the crowded environment as it experiences different types of interactions with the crowders. In addition, there exist other crucial factors such as activity, the density of crowders, heterogeneity, and the microarchitecture of the environment, which play a significant role in deciding the dynamics of the active probes in the crowded media. We portray how the translational and rotational dynamics of the active Janus particle change in a two-dimensional viscoelastic and non-viscoelastic environments with either attractive or repulsive interaction with the media.⁹ The Janus particle exhibits a nonmonotonic behavior in rotational dynamics with area fraction, while the translational dynamics monotonically decrease. Then we describe how the shape of the Janus probe affects the dynamics by investigating the translational and rotational dynamics of the self-driven rigid dumbbell in a 2D polymer gel.¹² Subsequently, the effect of confinement and crowding on the transport of the self-propelled spherical probe is discussed in detail by considering a spherical tracer in a polymer-grafted cylindrical channel.¹⁵ In general, we find that

the dynamics is qualitatively faster with increasing self-propulsion in all of these cases, but the magnitude of the enhancement depends on the architecture, crowding density, and interactions of the medium.

This review is organized as follows: section 2 describes the modeling and dynamical features of active Janus probe in polymeric as well as in colloidal solutions. Coupling–decoupling behavior of the active Janus probe with area fraction is included in section 3. Section 4 is devoted to dynamical changes happening to the chemically symmetric and asymmetric rigid dumbbell in 2D polymer gel, and section 5 presents the effect of the interplay of crowding and confinements on the dynamics of a spherical active probe particle inside the polymer grafted narrow cylindrical channel. Finally, section 6 summarizes the important aspects and indicates potential future research directions.

2. ACTIVE JANUS DIFFUSION IN POLYMER AND COLLOIDAL SOLUTIONS

Inspired by the remarkable performance of biological motors and pumps, researchers engineered function-specific hybrid biosynthetic nanomotors.¹⁶ A generic model of self-propelled swimmers is the well-celebrated active Brownian particle (ABP). The motion of the Janus probe in free space is well-studied. The translational and rotational dynamics of an active Janus particle show different dynamical features compared to the passive case. The translational dynamics display a steady three-step growth as short time diffusion, intermediate superdiffusion, and an enhanced diffusion at a long-time limit. However, the same Janus probe in the crowded medium has qualitatively different dynamics, where it frequently encounters crowders, and these crowders could be repulsive or sticky in nature. Further, to examine how the dynamics of swimmers change in crowded media, a minimalistic model of active Janus particle is modeled as a rigid body made of two spherical particles of the same size, separated by a constant distance ζ . This Janus particle is then introduced in a polymer solution, made up of N_p polymer chains, each consisting of M

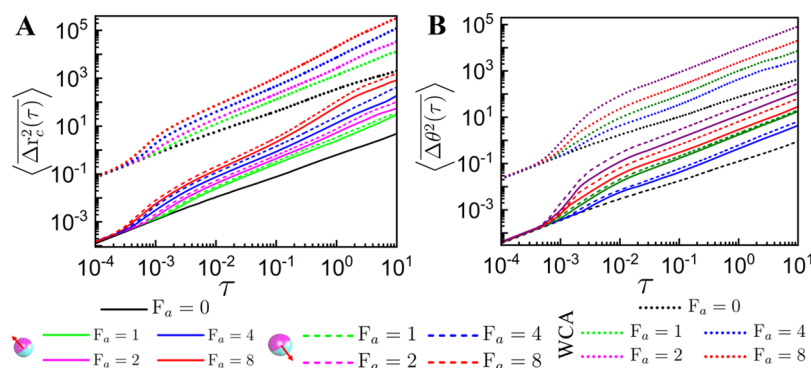


Figure 2. (A) Log–log plot of $\langle \Delta r_c^2(\tau) \rangle$ vs τ and (B) $\langle \Delta \theta^2(\tau) \rangle$ vs τ for the self-propelled Janus probe subjected to different F_a in purely repulsive polymers (dotted lines) and polymers with sticky zones (solid and dashed lines) ($\epsilon = 2.0$) for $\phi = 0.165$. In the plots, the solid and dashed lines represent the case with self-propulsion toward the sticky face and nonsticky face, respectively. Reproduced and customized with permission from ref 9. Copyright 2020 Royal Society of Chemistry.

= 100 beads (Figure 1A) or in a nonviscoelastic environment, composed of only monomers, which we refer to as colloids (Figure 1B). The viscoelastic crowders are modeled as colloidal beads connected by finitely extensible nonlinear elastic potential:

$$V_{\text{FENE}}(r) = \begin{cases} -\frac{k_f r_{\text{max}}^2}{2} \ln \left[1 - \left(\frac{r_{ij}}{r_{\text{max}}} \right)^2 \right], & \text{if } r_{ij} \leq r_{\text{max}} \\ = \infty, & \text{otherwise} \end{cases} \quad (1)$$

where r_{ij} is the distance between two neighboring monomers in the polymer chain with a maximum extension r_{max} , and k_f is the spring constant. To implement a nonviscoelastic crowded environment, the medium is filled with disconnected monomers (colloids) (Figure 1B). A pair of monomers, either free or connected, interact via repulsive Weeks–Chandler–Andersen (WCA) potential:¹⁷

$$V_{\text{WCA}}(r) = \begin{cases} 4\epsilon_{ij} \left[\left(\frac{\sigma_{ij}}{r_{ij}} \right)^{12} - \left(\frac{\sigma_{ij}}{r_{ij}} \right)^6 \right] + \epsilon_{ij}, & \text{if } r_{ij} < 2^{1/6} \sigma_{ij} \\ 0, & \text{otherwise} \end{cases} \quad (2)$$

where r_{ij} is the separation between a pair of monomers in the medium, ϵ_{ij} is the strength of the interaction, and σ_{ij} determines the effective interaction diameter. For a medium of nonadhesive (nonsticky) crowders, the interaction between both halves of the Janus probe and the polymers is modeled by the WCA potential (eq 2). On the other hand, each spherical particle in the Janus probe can interact differently with the monomers in the medium. Here, the probe is called the Janus particle, where one-half of the Janus is nonsticky, while the other is sticky which interacts repulsively (Figure 1C,D) via WCA potential (eq 2) and attractively via the Lennard-Jones (LJ) potential:

$$V_{\text{LJ}}(r) = \begin{cases} 4\epsilon_{ij} \left[\left(\frac{\sigma_{ij}}{r_{ij}} \right)^{12} - \left(\frac{\sigma_{ij}}{r_{ij}} \right)^6 \right], & \text{if } r_{ij} \leq r_{\text{cut}} \\ 0, & \text{otherwise} \end{cases} \quad (3)$$

where r_{ij} is the separation between the “sticky” monomers and the attractive part of the Janus probe, ϵ_{ij} is the strength of the interaction with an interaction diameter $\sigma_{ij} = \sigma_{\text{JN}}$, and the Lennard-Jones cutoff length $r_{\text{cut}} = 2.5\sigma_{\text{JN}}$. The other (non-adhesive) half of the Janus probe interacts repulsively with all of the monomers via the WCA potential (eq 2) but with interaction diameter σ_{JN} . Also, with the nonadhesive monomers (red in Figure 1A,B), both particles in the Janus probe interact via the WCA potential with the interaction diameter σ_{JN} . The energy is measured in terms of thermal energy $k_{\text{B}}T$, and we consider $\epsilon = 2$ according to this unit. The interaction diameter is $\sigma_{\text{JN}} = 1.25\sigma$, where σ is the unit of length. For all simulations, the Lennard-Jones parameters (σ and ϵ) and mass m are the fundamental units of length, energy, and mass, respectively. Therefore, the unit of time is $\tau = \sqrt{\frac{m\sigma^2}{\epsilon}}$. The Janus particle parameter is $\zeta = 0.6$ so that its shape anisotropy is not significant. The area fraction (ϕ) is defined as $\phi = \frac{N\pi\sigma^2}{4L_x \times L_y}$, where $N = N_p \times M$ is the total number of particles in the medium with diameter σ , and L_x and L_y are the lengths of the simulation box.

The dynamics of all of the particles in the system with mass m and position $\mathbf{r}_i(t)$ at time t are simulated using the following Langevin equation:

$$m_i \frac{d^2 \mathbf{r}_i(t)}{dt^2} = -\gamma \frac{d\mathbf{r}_i}{dt} - \sum_j \nabla V(\mathbf{r}_i - \mathbf{r}_j) + \mathbf{f}_i(t) + \mathbf{f}^{\text{act}} \quad (4)$$

Here, \mathbf{r}_j represents the position of all of the particles except the i th particle, $V(r) = V_{\text{LJ}} + V_{\text{WCA}} + V_{\text{FENE}}$, and is the resultant pair potential between the i th and j th particle. Note that $V_{\text{LJ}} = 0$ for purely repulsive interactions, $V_{\text{WCA}} = 0$ for attractive interactions, and $V_{\text{FENE}} = 0$ for free colloids in the environment. γ is the friction coefficient which is related to the Gaussian noise through

$$\langle f_\alpha(t) \rangle = 0, \quad \langle f_\alpha(t') f_\beta(t'') \rangle = 2d\gamma k_{\text{B}} T \delta_{\alpha\beta} \delta(t' - t'') \quad (5)$$

where k_{B} is the Boltzmann constant, T is the temperature, δ represents the Dirac delta function, α and β represent the Cartesian components, and d is the dimensionality. The term \mathbf{f}^{act} denotes the self-propulsion term for the active particles. For Janus particles, $\mathbf{f}_i^{\text{act}} = F_a \mathbf{n}$ in eq 4, where F_a is the strength of the propulsion force and \mathbf{n} is the unit connecting vector

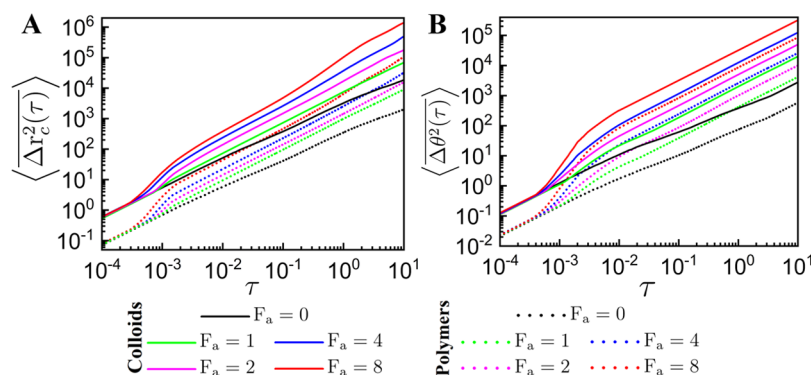


Figure 3. (A) Log–log plot of $\langle \Delta r_c^2(\tau) \rangle$ vs τ and (B) $\langle \Delta \theta^2(\tau) \rangle$ vs τ for the self-propelled Janus probe in the purely repulsive polymers (dotted lines) and in purely repulsive colloids (solid lines) for $\phi = 0.165$. Reproduced and customized with permission from ref 9. Copyright 2020 Royal Society of Chemistry.

between the two centers of the Janus probe. For passive monomers in the crowded environment, we set $F_a = 0$. All of the simulations are performed using LAMMPS,¹⁸ employing the Langevin thermostat and equation of motion integrated using the velocity Verlet algorithm in each time step.

The dynamics of a free particle is well-described in the literature.¹ The passive free Janus probe is diffusive at all times, whereas the free self-propelled Janus probe shows an enhanced translational mean square displacement ($\langle \Delta r_c^2(\tau) \rangle$), with distinct three regions: short-time diffusion, intermediate superdiffusion, followed by long-time diffusion with an enhanced diffusion coefficient. However, the rotational dynamics $\langle \Delta \theta^2(\tau) \rangle$ remains unaffected by self-propulsion as the rotational motion is solely governed by the thermal fluctuations. Hence, the persistence time, τ_R is the same for all values of F_a when crowders are not present in the medium. When the polymers are introduced in the media, the dynamics show entirely different behavior compared to the Janus probe in free space.⁹ In order to see the effect of interaction between the Janus probe and the crowders, the area fraction of the polymers is kept constant at $\phi = 0.165$. In one set of simulations, both the Janus halves interact repulsively with the monomers of the polymers. The passive Janus displays intermediate subdiffusion due to the presence of transiently surrounded polymers and achieves the diffusive limit at longer times (Figure 2A). However, for the active Janus probe, the self-propulsion helps the Janus probe to escape from the steric barrier created by these polymers, and $\langle \Delta r_c^2(\tau) \rangle$ shows a three-step growth similar to free self-propelled Janus probe, unlike that of a passive Janus probe in repulsive polymers (Figure 2A). Surprisingly, the presence of polymers results a three-step growth in $\langle \Delta \theta^2(\tau) \rangle$ similar to $\langle \Delta r_c^2(\tau) \rangle$, unlike a free self-propelled Janus probe (Figure 2B). When the self-propulsion F_a increases, both translational and rotational dynamics steadily increase, and this implies that the activity always helps the Janus probe to escape from the polymer chain cavities compared to the passive case. A similar trend in rotational dynamics has been observed by Gomez-Solano et al. in an experiment where they notice an enhanced diffusion in $\langle \Delta \theta^2(\tau) \rangle$ for a self-propelled Janus probe in a viscoelastic environment,⁶ when compared to the passive Janus particle. However, in their study, the Janus probe was much bigger than the polymers in the solution. Du et al. investigated the active Brownian particle diffusion in polymer solutions in 3D using

computer simulations.²² They reported a nonmonotonic dependence of the long-time diffusion coefficient on the particle size. They propose that the nontrivial dependence results from the competition between persistent motion of the active Brownian particle and the length-scale-dependent effective viscosity that the particle experiences in the polymer solution.²²

Next, the binding zone is introduced on the polymer chain by making the central beads attractive to one-half of the Janus probe, while the other half interacts repulsively with all of the monomers. The translational and rotational dynamics slow down due to the sticky zone and show a strong intermediate subdiffusion compared to the Janus probe in the purely repulsive polymer solution (Figure 2). The Janus probe is pulled in by the sticky zones of the polymers, which leads to this overall decrease in $\langle \Delta r_c^2(\tau) \rangle$ and $\langle \Delta \theta^2(\tau) \rangle$ compared to the purely repulsive polymer solution. However, this reveals that the presence of viscoelastic polymers results enhancement of rotational dynamics as a function of increasing activity, unlike the free Janus case where the rotation is independent of the activity. The local heterogeneity persists within a length scale comparable to the probe size, and the direction of propulsion of the Janus probe relative to its sticky face plays a crucial role in controlling the dynamics. The direction of self-propulsion toward the nonsticky face (Figure 1C) facilitates faster translation and rotation compared to the case where the direction of self-propulsion points toward the sticky face (Figure 1D) (the dashed and solid lines, respectively, in Figure 2). This depicts that the self-propulsion outward from the nonsticky face helps in escaping from the sticky traps created by the polymer chains. The qualitative trend remains the same for the nonviscoelastic crowders (colloids) obtained by removing the bond connecting the monomers of the polymers but shows faster translational and rotational dynamics of the Janus for a fixed F_a (Figure 3). This implies that the viscoelasticity is not a necessary condition to see enhancement in rotational dynamics compared to a free Janus probe. The dynamics is faster in colloidal solutions than the viscoelastic polymers. The origin of the rotational enhancement observed is due to the additional torque arising from the activity-dependent interactions between the Janus probe and the passive crowders. Since the monomers are connected in the viscoelastic case, the motion of individual polymer beads is constrained compared to that of the free colloidal beads. In a viscoelastic environment, the Janus probe is restricted inside

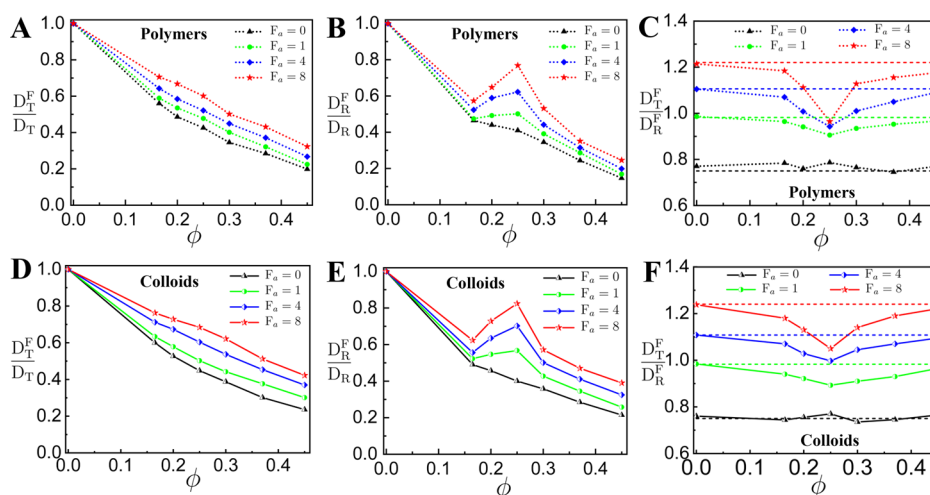


Figure 4. Normalized translational, rotational diffusion coefficients, $\frac{D_T^F}{D_R^F}$ and $\frac{D_R^F}{D_T^F}$, respectively, and the ratio of diffusivities, $\frac{D_T^F}{D_R^F}$, for the self-propelled Janus probe in different area fractions ϕ of the polymers having sticky zones ($\epsilon = 2.0$) (A–C) and binary mixture of attractive ($\epsilon = 2.0$) and repulsive colloids (D–F) for different F_a . Reproduced and customized with permission from ref 9. Copyright 2020 Royal Society of Chemistry.

cavities created by long chains leading to a diminution of diffusivity compared to the colloid crowders. In support of our studies, it has been recently shown that in a bath of passive silica tracers, tagged self-propelled Janus particles show enhancement in rotational dynamics with an increase in self-propulsion force.⁷ However, they did not capture any nonmonotonic variation of rotational dynamics of the active Janus with the area fraction of the bath particles.

3. COUPLING–DECOUPLING OF TRANSLATIONAL AND ROTATIONAL DYNAMICS OF JANUS PROBE IN CROWDED MEDIA

One of the crucial factors that decides the motion of a probe particle in crowded media is the crowding density. The architecture of the media, available free space, and the interactions from the surrounding particles essentially depend on the crowding density. For a two-dimensional system, the crowding density is quantified using the area fraction (ϕ). The area fraction is varied by keeping F_a constant, and it is found that the translational motion monotonically decreases, while the rotational dynamics interestingly shows a nonmonotonic behavior with increasing area fraction (Figure 4). The rotational diffusivity increases up to intermediate ϕ and then decreases for larger ϕ (Figure 4B,E). The nonmonotonic behavior in the motion leads to coupling or decoupling between the translational and rotational dynamics. The translational and rotational diffusions remain coupled as long as the ratio of the respective diffusion coefficients remains constant. The rotation of a free Janus particle is purely governed by the thermal diffusion, thus the ratio of translational and rotational diffusion coefficients ($\frac{D_T^F}{D_R^F}$) is a constant. However, any deviation of this ratio from the constant value should result from the decoupling of translational and rotational motions.¹⁹ This is a sophisticated way to determine the coupling and decoupling behavior of the dynamics of the Janus probe. The coupling and decoupling between the translational and rotational dynamics were reported previously by Edmond et al. in an experimental study of the dynamics of the tetrahedral tracer colloidal

clusters in a dense amorphous suspension of colloidal spheres using high-speed confocal microscopy.¹⁹ Similarly, Zou et al. observed a coupling–decoupling behavior in translational and rotational diffusion of glass-forming liquid of monodisperse soft Janus particles near the glass transition temperature, though for a passive system.²⁰ Spatial heterogeneity in the medium results in such a decoupling.²⁰ Thus, for a free self-propelled Janus particle, translational and rotational motions are always coupled. The behavior changes in the crowded media. For the passive Janus probe ($F_a = 0$), the ratio of translational and rotational diffusivity of Janus probe in the presence of crowders $\frac{D_T^F}{D_R^F}$ became independent of ϕ , indicating a coupling between translational and rotational diffusion at all densities. However, the active Janus probe exhibits intriguing change as the diffusivity ratio shows a strong dependence of ϕ , as it shows a minimum at intermediate ϕ . This behavior becomes more pronounced for higher values of F_a (Figure 4C,F). For larger ϕ , the ratio approaches the free Janus value. The decoupling behavior is due to the nonmonotonic changes in the rotational dynamics of the Janus probe. The Janus probe is surrounded by obstacles, and the mean free path of the probe decreases with increasing ϕ . The reorientation events also change the direction of motion, and the Janus probe with enhanced diffusivity translates to a different location followed by the rotation as it encounters the obstacles. These interactions lead to further random rotation and result in increased rotational diffusivity as a function of F_a at smaller ϕ . At larger ϕ , these rotations get suppressed as sufficient free space is not available for the probe to rotate owing to the crowding. On the other hand, the translational diffusivity decreases monotonically with increasing ϕ , as the translational motion gets suppressed due to the steric hindrance coming from the obstacles. Altogether, the physics describing the enhancement in translational and rotational dynamics of the Janus probe provides a detailed understanding of the transport of the self-powered machines through complex media, where it encounters multiple interactions and competing factors.

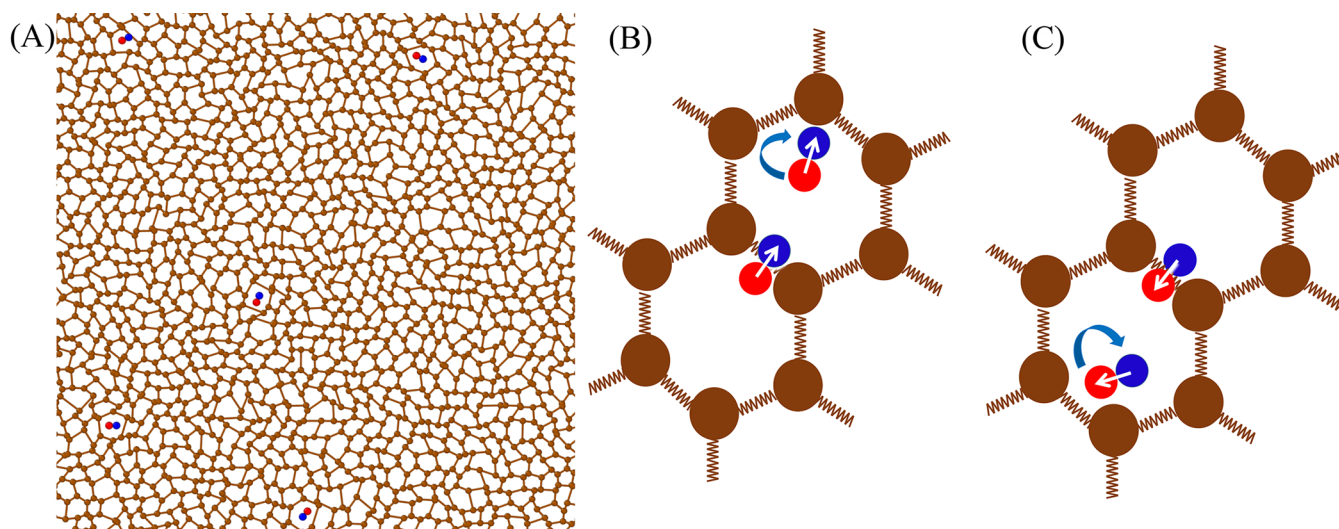


Figure 5. (A) Snapshot of chemically asymmetric self-driven rigid dumbbells inside the polymer gel (brown color; springs are shown as solid lines). A schematic representation of (B) trapping, rotation, and (C) mesh-to-mesh transition events of the self-driven rigid dumbbells in the polymer gel. The white arrows indicate the direction of self-propulsion. Reproduced and customized with permission from ref 12. Copyright 2022 Royal Society of Chemistry.

4. SELF-DRIVEN RIGID DUMBBELLS IN POLYMER GEL

Understanding the motion of the probe particle in the crowded medium is imperative in designing self-propelled artificial devices which can be used as a potential candidate for targeted drug delivery in crowded¹⁶ and heterogeneous environments like biological cells. There exist a series of factors that control the transport of these microswimmers through the crowded space. The interplay between the shape, interactions, and self-propulsion determines how efficiently a probe moves through the dense space. Further, to understand how the asymmetry of the Janus probe impacts the transport in a crowded environment, a chemically symmetric and asymmetric self-driven rigid dumbbell in polymer gel was created on a 2D lattice (Figure 5). The translational and rotational dynamics of the self-driven rigid dumbbells were investigated to unveil the impact of chemical symmetry or asymmetry on the transport of an active extended Janus particle through dense polymeric gel media. Macromolecular crowding plays a vital role in deciding the motion of active agents through physiological environments, such as living cells, where the biomolecules are transported through the networks formed by biofilaments or molecules diffusing through the chromatin networks inside the eukaryotic nuclei. The biomolecular transport depends on the effective diffusion of biological swimmers. These probes, while moving through the confined dense space, encounter frequent collisions and interact intensely with the crowd. To mimic these microswimmers in crowded space, a self-driven rigid dumbbell is modeled by connecting two circular discs each of size 0.5σ via harmonic spring potential.

$$V_{\text{harmonic}}(r_{ij}) = k_H \frac{(r_{ij} - r_0)^2}{2} \quad (6)$$

Here, $k_H = 30$ is the spring constant, and r_0 is the equilibrium distance between the two halves of the rigid dumbbell ($\delta l = 0.5\sigma$), which is constant throughout the simulations, and it ensures that the dimers are always translating and rotating as a single rigid body. Next, the crowded environment is modeled by creating a bead–spring polymer gel on a 2D graphene lattice, and each of these trivalent lattice sites is occupied by

monomers of the same diameter, σ (Figure 5), and are connected to the neighboring monomers through the finitely extensible nonlinear elastic (FENE) spring potential (eq 1). The distance r_{ij} between two neighboring monomers in the polymer gel with a maximum length $r_{\text{max}} = 2.5\sigma$ and $k_f = 3$ is the force constant, which accounts for the stiffness of the gel. The nonbonded gel monomer–monomer, two halves of the rigid dumbbells, and the rigid dumbbell with the monomers of the polymer gel interactions is set as purely repulsive and modeled by the Weeks–Chandler–Andersen (WCA) potential (eq 2).¹⁷ In this case, the rigid dumbbell is chemically symmetric as both the halves interact similarly to the crowd. Further, the chemical asymmetry is achieved by making one-half of the dumbbell interact attractively with the monomers of the polymer gel via the Lennard-Jones potential (eq 3). Here, r_{ij} is the separation between one-half of the rigid dumbbell and monomers of the gel, ϵ is the strength of the interaction (stickiness) with an interaction diameter σ_{ij} , and the Lennard-Jones cutoff length $r_{\text{cut}} = 2.5\sigma$.

The Langevin equation (eq 4) is implemented to describe the dynamics of a particle with mass m and position $r_i(t)$ at time t , interacting with all of the other particles in the system. In eq 4, m is the mass of particles, $r_i(t)$ is the position of i th particle at time t , γ is the friction coefficient, and the total potential energy of the system can be written as $V(r) = V_{\text{FENE}} + V_{\text{harmonic}} + V_{\text{LJ}} + V_{\text{WCA}}$, where V_{FENE} is the spring potential for the polymer gel, V_{harmonic} is the spring potential connecting two halves of the rigid dumbbell, V_{LJ} is the attractive potential, and V_{WCA} corresponds to the excluded volume potential. Thermal fluctuations are captured by the Gaussian random force $f_i(\ell)$, satisfying the fluctuation–dissipation theorem given by eq 5. The activity is modeled as a propulsive force $F_a \mathbf{n}$, where F_a represents the amplitude of active force with the orientation specified by the unit vector \mathbf{n} connecting the centers of the two spherical discs which form the rigid dumbbell. The self-propulsion term $F_a \mathbf{n}$ is zero for the passive polymer gel particles. In the case of the asymmetric dumbbell, two directions of self-propulsion are considered, either outward from the sticky face or nonsticky face, but acting always along

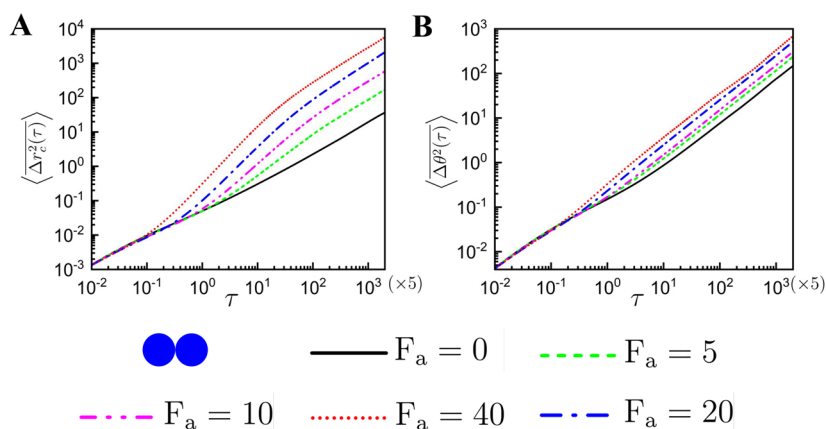


Figure 6. Log–log plot of (A) $\langle \Delta r_c^2(\tau) \rangle$ vs τ and (B) $\langle \Delta \theta^2(\tau) \rangle$ vs τ of the attractive ($\epsilon = 1.0$) self-driven symmetric dumbbell in 2D polymer gel for different F_a . Reproduced and customized with permission from ref 12. Copyright 2022 Royal Society of Chemistry.

the bond. The activity is expressed in terms of a dimensionless quantity Péclet number, Pe defined as $Pe = \frac{F_a \sigma}{k_B T}$. Therefore, $F_a = 0$ corresponds to the passive case. For each simulation, the system is initialized by randomly placing five self-driven rigid dumbbells inside the polymer gel packed inside a square box of length 52σ (Figure 5). Periodic boundary conditions are set in all directions. All of the simulations are performed using the Langevin thermostat, and the equation of motion (eq 4) is integrated using the velocity Verlet algorithm in each time step. All production simulations were carried out for 5×10^8 steps after relaxing the system long enough where the integration time step was considered to be 5×10^{-4} and the positions of the particles were saved every 100th step. This also ensures the equilibration of the polymer gel with an average mesh size $\sigma_{\text{mesh}} \approx 1.7\sigma$.

To understand the dynamical properties of the rigid dumbbell, the time-ensemble-averaged translational and rotational mean square displacements, $\langle \Delta r_c^2(\tau) \rangle$ and $\langle \Delta \theta^2(\tau) \rangle$, are computed. Here, r_c is the center of mass position and θ is the angle between x -axis and body axis of the dumbbell.¹² For computing $\langle \Delta \theta^2(\tau) \rangle$, the cumulative angle θ is calculated from the simulation; therefore, the angle difference is no longer bounded by 2π .⁸ A chemically symmetric dumbbell with both halves sticky ($\epsilon = 1$) to the monomers of the polymer gel is considered and investigated for the effect of self-propulsion on its transport inside the polymer gel. The self-propulsion always results in faster dynamics with increasing F_a , as shown in Figure 6. $\langle \Delta r_c^2(\tau) \rangle$ shows a short-time subdiffusion as the symmetric dumbbell gets caged inside the polymer mesh due to the stickiness between the dumbbell and the polymer gel. At intermediate time, the subdiffusive behavior becomes more pronounced for the passive case, while $\langle \Delta r_c^2(\tau) \rangle$ for the self-driven symmetric dumbbell grows faster as a function of increasing F_a (Figure 6). Also, for smaller activities, the self-driven symmetric dumbbell shows a subdiffusive behavior owing to the confined motion inside the polymer mesh for a very short time. As time progresses, activity dominates and performs a persistent motion, which results in superdiffusive behavior. At the longer time, the directed motion is randomized due to the collisions and reorients, which help the symmetric dumbbell to reach the diffusive limit; that is, $\langle \Delta r_c^2(\tau) \rangle$ is linear in time with an enhanced diffusion

coefficient. Self-propulsion helps the symmetric dumbbell to make a series of transitions between the meshes and explore a larger space inside the gel. Further, to unravel the effect of self-propulsion, crowding, and the stickiness of the network particles on the rotational dynamics of the symmetric dumbbell, $\langle \Delta \theta^2(\tau) \rangle$ is computed as a function of activity F_a (Figure 6B). An activity-induced splitting of $\langle \Delta \theta^2(\tau) \rangle$ curves (Figure 6) is observed for the symmetric dumbbell inside the polymer gel, unlike the self-driven probe in free space. Similar to translational motion, $\langle \Delta \theta^2(\tau) \rangle$ also shows enhancement with increasing the self-propulsion. At the intermediate time, $\langle \Delta \theta^2(\tau) \rangle$ exhibits a subdiffusive behavior, which is more prominent for the passive as well as for the smaller F_a values, and at higher F_a , the subdiffusion changes to superdiffusion (Figure 6B). At longer time, $\langle \Delta \theta^2(\tau) \rangle$ displays the diffusive behavior with an enhanced diffusion coefficient. The self-propelled dumbbell encounters the polymer gel particles more frequently and undergoes frequent rotations. This results from the additional activity-induced torque responsible for the enhancement in rotational motion of the self-driven dumbbell compared to the passive dumbbell. When the dumbbell is self-propelled, it has faster translational motion and also while moving encounters the gel particles more frequently than when it is passive. Since the probe is asymmetric in shape, it undergoes rotations while colliding with the gel monomers. A self-propelled dumbbell undergoes more frequent rotations, resulting from the torque generated by interacting with the medium, which increases with the magnitude of the self-propulsion.

The chemically symmetric dumbbells have identical faces. But to obtain a better understanding of the role of the chemistry of the probe, one has to consider the probe as a chemically asymmetric particle, which is achieved by introducing repulsive and sticky interactions on the two different halves of the rigid dumbbell. Here, the direction of self-propulsion also plays a crucial role, like the self-propelled Janus probe. The effects of chemical asymmetry and direction of self-propulsion on the dynamics of the rigid dumbbell are studied by comparing it with the chemically symmetric dumbbell. $\langle \Delta r_c^2(\tau) \rangle$ and $\langle \Delta \theta^2(\tau) \rangle$ for the chemically asymmetric dumbbell show enhancement in both translational and rotational dynamics with qualitatively similar trends in

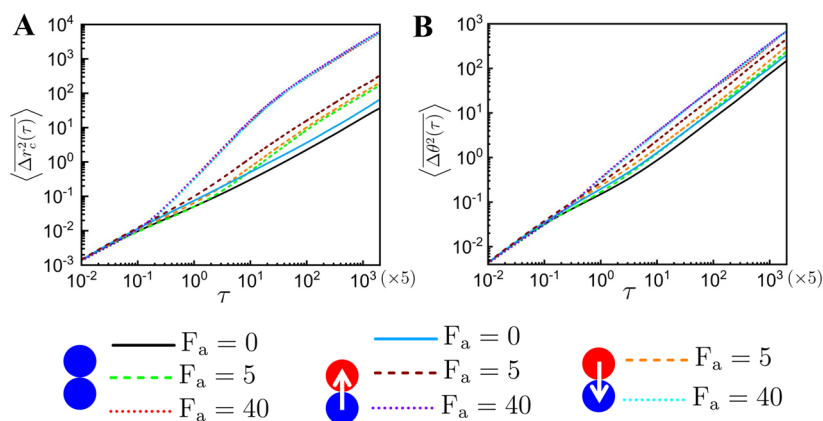


Figure 7. Log–log plot of (A) $\langle \Delta r_c^2(\tau) \rangle$ and (B) $\langle \Delta \theta^2(\tau) \rangle$ vs the lag time τ of the passive and self-driven sticky ($\epsilon = 1.0$) symmetric dumbbell, asymmetric dumbbell with self-propulsion along the sticky half, and self-propulsion along the nonsticky half in 2D polymer gel for different F_a . Reproduced and customized with permission from ref 12. Copyright 2022 Royal Society of Chemistry.

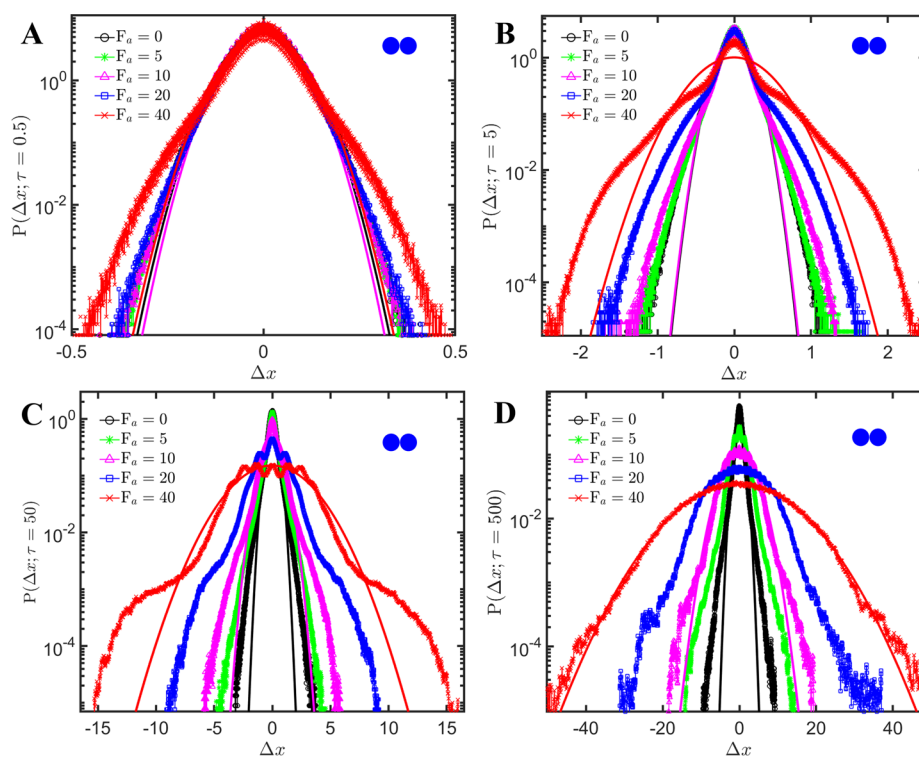


Figure 8. Plots of $P(\Delta x; \tau)$ for the symmetric sticky ($\epsilon = 1.0$) dumbbell as a function of F_a at different lag times τ (0.5, 5, 50, and 500) (A–D). The solid lines represent the Gaussian fittings. Reproduced and customized with permission from ref 12. Copyright 2022 Royal Society of Chemistry.

comparison to the symmetric case (Figure 7). The symmetric dumbbell gets trapped inside the polymer gel due to the higher effective sticky interaction coming from the two halves of the dumbbell having an attractive interaction with the gel, while for the asymmetric dumbbell, one-half interacts repulsively with the polymer gel and reduces the chances of getting caged in the dense polymer gel. Apart from this, if the direction of self-propulsion is toward the nonsticky half of the asymmetric dumbbell, it always facilitates the escape of the dumbbell from the polymer mesh traps (Figure 5C). Thus, the asymmetric case exhibits enhanced translational and rotational dynamics compared to their symmetric counterpart (Figure 7). The enhanced rotation is due to the extra torque that arises from the force imbalance due to simultaneous repulsive and attractive interactions experienced by the two halves of the

chemically asymmetric rigid dumbbell compared to the symmetric case. The directional effect has already been reported previously for a self-propelled Janus probe.⁹ However, at very high F_a , the activity dominates and the chemical asymmetry or the direction of self-propulsion does no longer have any effect on the dynamics of the rigid dumbbell as the $\langle \Delta r_c^2(\tau) \rangle$ and $\langle \Delta \theta^2(\tau) \rangle$ curves are indistinguishable from each other for $F_a = 40$ (Figure 7). Recently, Klett et al. studied the self-diffusion of flexible passive dumbbells in crowded two-dimensional solutions.⁸ They focused on the effects of the crowding fraction and of the particle structure on the diffusion characteristics. They reported that the crowded system of dimers exhibits two distinct diffusion regimes attributed to the crowding-induced transition from a purely viscous to a

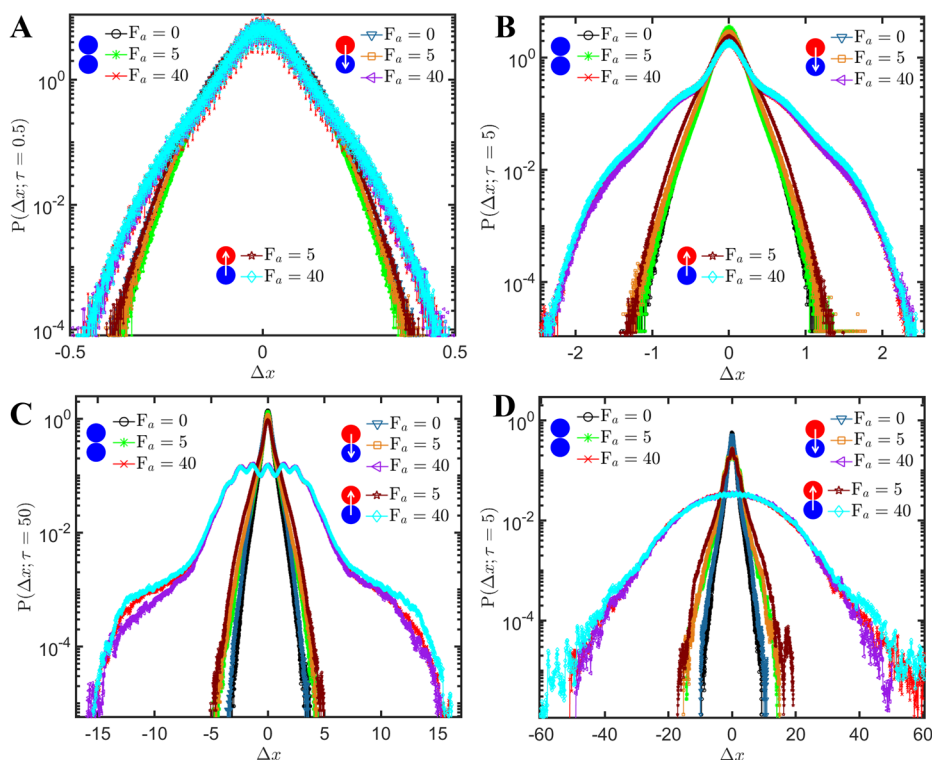


Figure 9. Plots of $P(\Delta x; \tau)$ for the comparison of asymmetric dumbbell with self-propulsion along the sticky ($\epsilon = 1.0$) half (arrow toward blue half), self-propulsion along the nonsticky half (arrow toward red half), and symmetric dumbbell in the polymer gel for $F_a = 0, 5,$ and 40 at different lag times τ ($0.5, 5, 50,$ and 500) (A–D). Reproduced and customized with permission from ref 12. Copyright 2022 Royal Society of Chemistry.

viscoelastic behavior of the diffusion environment upon increasing crowding fraction.⁸ We consider a rigid dumbbell in the polymer network, and hence our model differs from their system in terms of the dumbbell properties and density of crowders.

4.1. Mesh-to-Mesh Motion of a Self-Driven Rigid Dumbbell inside the Polymer Gel. It is important to understand how the rigid dumbbell moves through the polymer gel as the gel contains the small connected mesh-like architecture that controls the diffusion of particles. One of the standard methods to capture the nature and behavior of the diffusion of probe particles is using the van Hove correlation function, $P(\Delta x; \tau)$. The self-part of the van Hove correlation is calculated as $P(\Delta x; \tau) \equiv \langle \delta(\Delta x - (x(t + \tau) - x(t))) \rangle$ of the dumbbell displacement in one dimension (along the x -direction in this case). This analysis can provide insights on the Gaussian and non-Gaussian nature of the diffusion at short, intermediate, and long times. This done by fitting respective $P(\Delta x; \tau)$ with the corresponding Gaussian distribution fittings for the Brownian motion,

$$P(\Delta x; \tau) = \frac{1}{\sqrt{2\pi\langle\Delta x^2\rangle}} \exp\left(-\frac{\Delta x^2}{2\langle\Delta x^2\rangle}\right)^{8,12,15}$$

At very short time, the $P(\Delta x; \tau)$ of the symmetric dumbbell curves merge for smaller F_a , and the distributions become broader for larger values of F_a (Figure 8). As time progresses, the dumbbell explores more space inside the gel, and $P(\Delta x; \tau)$ becomes broader with increasing activity. At intermediate time, $P(\Delta x; \tau)$ exhibits central multiple peaks with increasing F_a (Figure 8). The observed behavior is due to the adjacent mesh-to-mesh motion of the self-driven dumbbell. In general, the active probe in confinement tends to move toward the boundary of the confinement to escape if there is a chance. Thus, the

occurrence of multiple central peaks is a characteristic of the mesh-to-mesh motion of the dumbbell. Similarly, multiple central peaks in the van Hove function were reported previously in theoretical studies of tracer particle dynamics in an elastic active gel.²¹ More recently, such side peaks were observed in experiments involving tracer particles in an active gel. The activity was caused by the plasmodial oscillation of the slime mold *Physarum polycephalum*.¹⁴ Further, increasing F_a results in more numbers of central peaks, as the self-propulsion facilitates the mesh-to-mesh motion of the dumbbell (Figure 8). In the long-time limit, the density profile broadens due to the diffusive motion of the self-driven dumbbell. For the passive case, the distribution fitted well and $P(\Delta x; \tau)$ curves start deviating from Gaussianity with increasing F_a and is more prominent at the intermediate time limit. At long times, the self-driven dumbbell reaches the diffusive regime, and the distributions exhibit Gaussianity (Figure 8). The asymmetric dumbbell also exhibits a qualitatively similar trend in the density profile, but $P(\Delta x; \tau)$ curves are more broadened compared to the symmetric counterpart (Figure 9). Also, the directional effects persist here, as well, like the previous case.⁹ The self-propulsion toward the nonsticky half has a broader distribution than the sticky half and the symmetric dumbbell. The self-propulsion toward the sticky half promotes trapping, while self-propulsion along the nonsticky half helps in escaping the asymmetric dumbbell, causing the $P(\Delta x; \tau)$ distribution to be broader. However, at very high F_a , the activity dominates over the chemical asymmetric effects, and direction of propulsion force leads to the distribution curves merging and falling on top of each other (Figure 9).

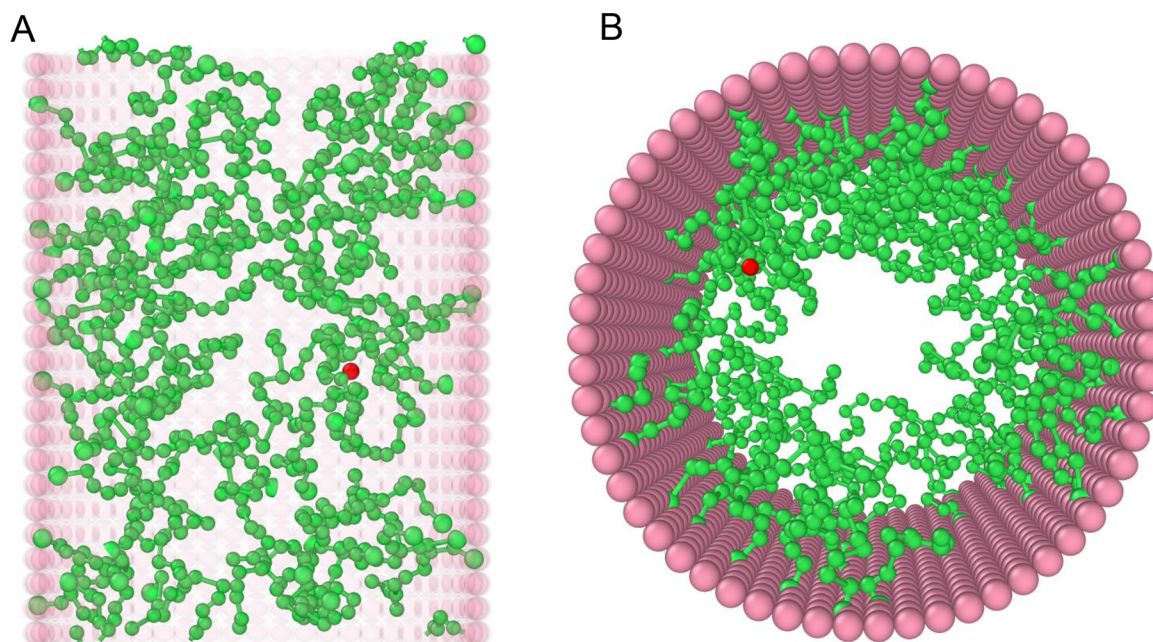


Figure 10. (A) Top view and (B) side view of the snapshot of a representative tracer particle (red) inside the polymer (green) grafted cylindrical channel with rigid walls (magenta). The wall particles are made transparent in the side view to show the grafted polymers clearly. Here, the size of the tracer is the same as that of a monomer. Reproduced and customized with permission from ref 15. Copyright 2022 Royal Society of Chemistry.

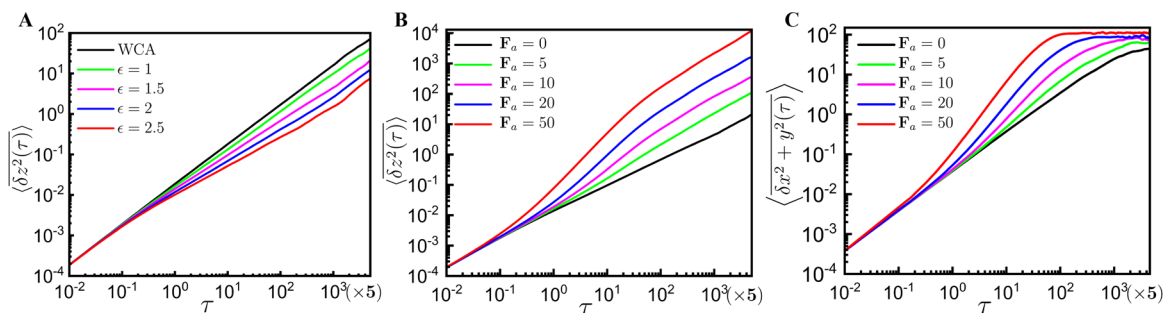


Figure 11. Log–log plot of $\langle \delta z^2(\tau) \rangle$ vs τ for the (A) passive tracer particle at different ϵ , (B) self-propelled tracer at different F_a , and (C) $\langle \delta x^2 + \delta y^2(\tau) \rangle$ vs τ at different F_a in the polymer-grafted cylindrical channel. Reproduced and customized with permission from ref 15. Copyright 2022 Royal Society of Chemistry.

5. ACTIVE PARTICLE TRANSPORT IN A POLYMER-GRAFTED CYLINDRICAL CHANNEL

The diffusion of probe particles of different length scales is always important in the context of biological processes. In cellular processes, the combined efforts of multiple factors maintain the smooth functioning of the cell and its biological functions. Thus, in real-life situations, there exist many factors that significantly affect the dynamics or the transportation of probe particles, such as activity, size, and shape of the probe particles, and its interactions with the local environment.^{9,12,13}

Among these processes, the macromolecular transport through the cellular channels in biological systems is of interest to researchers, where, along with crowding, confinement plays a crucial role. Cellular channels, like the nuclear pore complex (NPC), allow a bidirectional transport of ions and proteins across the nuclear envelope by passive diffusion through the channels. To investigate the dynamics of active agents through such a crowded channel, a spherical self-propelled particle in a cylindrical channel with polymers grafted on the inner wall is studied (Figure 10).¹⁵ The cylindrical channel of height 24σ and radius 9σ is grafted with a total of 75 polymer chains, each

containing 12 monomers of diameter σ , and is connected by FENE potential (eq 1) (Figure 10). The maximum displacement of the bond connecting the neighboring monomers is $r_{\max} = 5\sigma$ with the stiffness constant $k_f = 7$. The repulsive interactions between the polymer beads and the wall particles are modeled via the purely repulsive Weeks–Chandler–Andersen (WCA) potential (eq 2). For the case where the probe particle interacts attractively with the monomers of the grafted chain, it is modeled by the Lennard–Jones potential (eq 3).

The Langevin equation (eq 4) is implemented to simulate the dynamics of a particle with mass m and position $r_i(t)$ at time t , interacting with all the other particles in the system. The thermal fluctuations are captured by the Gaussian random force given by eq 5. Note that $F_a = 0$ for the passive particles. The activity term $\mathbf{f}^{\text{act}} = F_a \mathbf{n}$, which represents the magnitude of the active force F_a with orientation specified by the unit vector \mathbf{n} . The change in orientation follows $d\mathbf{n}/dt = \boldsymbol{\eta}(t) \times \mathbf{n}$, where $\boldsymbol{\eta}(t)$ is the Gaussian distributed stochastic vector with $\langle \boldsymbol{\eta}(t) \rangle = 0$ and time correlations given by $\langle \eta_\alpha(t') \eta_\beta(t'') \rangle = 2D_R \delta_{\alpha\beta} \delta(t' - t'')$, where D_R is the rotational diffusion

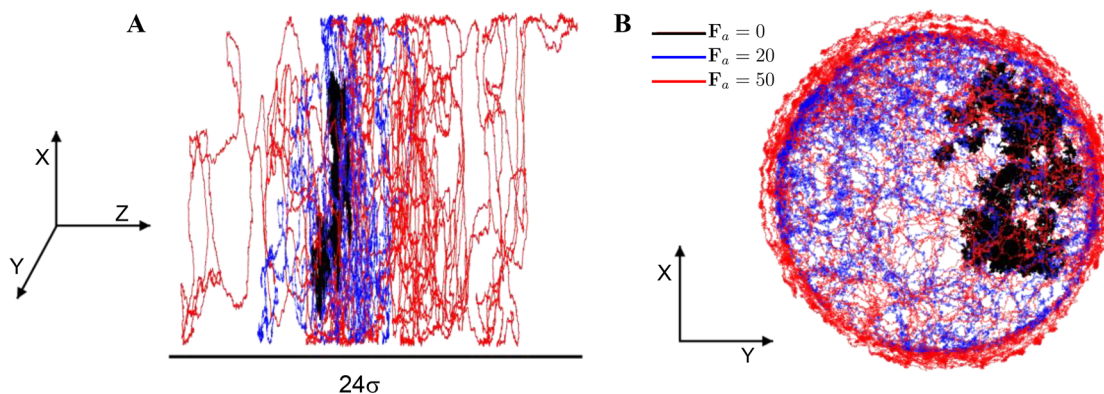


Figure 12. (A) Side view and (B) top view of the trajectory of the tracer particle in the polymer grafted cylindrical channel for different F_a . Reproduced and customized with permission from ref 15. Copyright 2022 Royal Society of Chemistry.

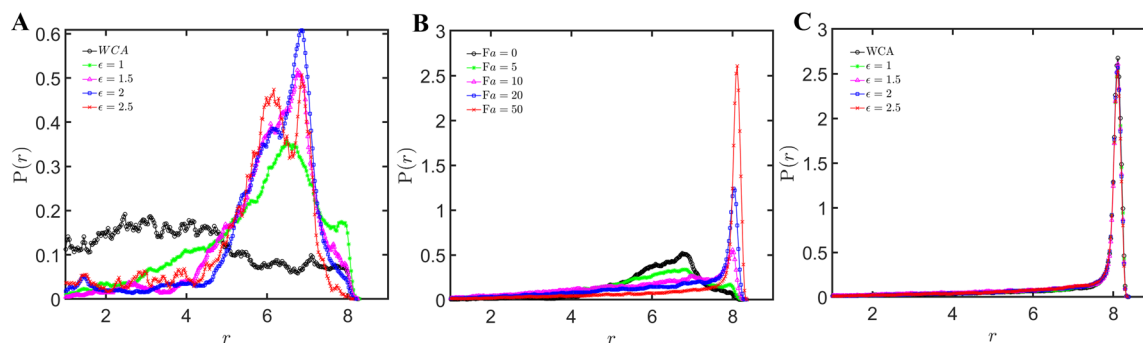


Figure 13. $P(r)$ of the tracer particle in the polymer-grafted cylindrical channel with (A) different ϵ for $F_a = 0$, (B) different F_a for $\epsilon = 1.5$, and (C) different ϵ for $F_a = 50$. Reproduced and customized with permission from ref 15. Copyright 2022 Royal Society of Chemistry.

coefficient. The unit vector \mathbf{n} can be expressed in the form of spherical coordinates.²² The system is equilibrated for 10^7 steps after placing the tracer inside the polymer-grafted cylinder. The simulations are carried out for 5×10^8 steps where the integration time step is considered to be 5×10^{-4} and the position of the tracer particle is recorded every 100th step.

The dynamical properties of the probe particle are quite different in the confined system compared to the same probe in free space. The confinements restrict the motion of the probe and provide this additional competing factor along with the self-propulsion, interactions, and crowding. In the narrow channel, the transport of the probe differs from the usual transport pathways as along the radial direction the confinement created by the cylindrical wall restricts the movement, while along the cylinder axis it is free to move. It is equally important to check how the dynamics changes along the radial directions where it encounters the wall as well as the cylinder axis (along the cylindrical axis a periodic boundary condition has been imposed) for obtaining a deeper understanding of the probe transport through the narrow channel. Initially the difference can be studied by analyzing the time-and-ensemble averaged translational mean square displacement of the probe along the cylinder axis ($\langle \delta z^2(\tau) \rangle$) as well as along the radial ($\langle \delta(x^2 + y^2)(\tau) \rangle$) directions as a function of lag time τ for different self-propulsion forces F_a (Figure 11B,C). The passive probe is subdiffusive inside the polymer-grafted cylindrical channel (Figure 11A). On the other hand, the motion of the self-propelled spherical probe in the cylindrical channel grafted with polymers shows a three-step growth in $\langle \delta z^2(\tau) \rangle$: short-

time normal diffusion, intermediate superdiffusion, and a long-time enhanced diffusion along cylinder direction (along the z -axis) similar to typical active Brownian particle as a function of increasing F_a (Figure 11B).¹⁵ However, the dynamics along the radial directions is quite different as $\langle \delta(x^2 + y^2)(\tau) \rangle$ exhibit a saturation at the long-time limit owing to the confinement created by the wall particles of the cylindrical channel (Figure 11C). This behavior is absent for smaller values of F_a , as the probe particle is not able to reach the wall of the cylinder to feel confinement.

Biological systems, such as cells, are heterogeneous, crowded, and have boundaries. Hence, the transport of agents through crowded confined spaces is imperative to understand the mechanism behind daily life activities. The importance of spherical probe transport through polymer-grafted cylindrical channel lies in this context. The interaction strength (stickiness), self-propulsion, grafting density, etc. play a vital role here. When the grafted polymers are purely repulsive (WCA), the passive probe prefers to move through the free pore-like space available between the grafted polymers along the cylinder axis, resulting in a diffusive behavior. However, when the probe and polymers possess an attractive interaction, the dynamics of the probe particle slows down as the tracer particle gets trapped inside the grafted polymeric zone, resulting in subdiffusive behavior at the intermediate time, which becomes more pronounced with increasing ϵ (Figure 11A).¹⁵ Making the probe self-propelled, the behavior changes as the self-propulsion turns the subdiffusion to superdiffusion at the intermediate time (Figure 11B). The activity helps the tracer particle to escape from the grafted polymeric zone, and the dynamics get faster with increasing F_a compared to the

passive counterpart. At higher F_a , the dynamics of the self-propelled tracer becomes much faster and frequently changes its directions as it repeatedly encounters the grafted polymer chains, loses the specificity, and goes deep into the grafted polymeric area near the wall of the cylinder (Figure 12). Consequently, the self-propelled particle explores most parts of the narrow channel by frequently changing the directions with higher F_a value (Figure 12).

The self-propelled probe covers most of the space inside the cylindrical channel, and the probability density $P(r)$ portrays the probe displacement along the radial directions where it encounters the grafted polymers. $P(r)$ gives the probability density of finding the tracer along the radial direction. For the purely repulsive passive probe, $P(r)$ is maximum at the cylindrical axis of the channel and gradually decreases toward the wall of the cylinder (Figure 13). This implies that the probe prefers to stay in the hollow pore-like space in the central region than the crowded polymeric zone. The density profile changes drastically when the probe is sticky to the polymers as $P(r)$ shows a maximum density at the grafted polymeric zone toward the wall region and a low density at the central region (Figure 13). The attractive interaction significantly drags the probe toward the grafted polymeric zone from the center, and the maxima shifts to larger values of r as a function of increasing r (Figure 13). When the probe is self-propelled, $P(r)$ shows more broader and flat density profile with increasing F_a . However, for a very high F_a range, the active probe prefers to stay close to the wall confinement which results in a narrow distribution. This is reflected irrespective of the stickiness as the probe spends more time close to the wall of the cylinder for all values of ϵ . It is equally probable to have the tracer everywhere inside the cylindrical channel for higher values of F_a . Adding to this, further insights on the probe dynamics are obtained from the analysis of the van Hove function. It is a standard tool for studying the Gaussian or non-Gaussian nature of the dynamics of the probe.^{12,15} The distribution becomes narrower with increasing ϵ and can be well-fitted by Gaussian distributions.¹⁵ In contrast, the dynamics shows a non-Gaussian behavior with a broader probability density profile as a function of increasing F_a due to the self-propelled motion of the probe.¹⁵ The self-propelled probe transport can provide useful insights into the active transport facilitated by biological pumps or motor molecules.¹⁶ A deeper understanding of the transport mechanism will help scientists to design hybrid biosynthetic nano- or micro-transporters by incorporating motor proteins into artificial systems.¹⁶

6. SUMMARY

We conclude this review by briefly highlighting the recent progress that enabled us to attain a better understanding of the dynamics of active probes in complex environments. We describe the transport of the active Janus probes in different environments and how the interactions, crowding density, nature of the media, activity, and the direction of self-propulsion influence the transport process. The translational dynamics exhibit a monotonic decay, while the rotational diffusion shows a nonmonotonic behavior with an increasing area fraction of the crowders. This further leads to a decoupling of translational and rotational dynamics at the intermediate area fractions. Then we portray how the chemical symmetric-asymmetric nature of the probe impacts the dynamics in dense media. The chemical asymmetry facilitates

the escape of the probes from the mesh confinement, and this results in a faster translational and rotational dynamics. Moreover, in addition to crowding the biological systems possess confinements. This provides additional complexity in understanding the dynamics of the probe particles. One has to consider the combined effect of confinements as well as the crowders to account for the transport mechanism in such a case. Here, we discuss how one can efficiently transport the active probe through a narrow channel where crowding, interactions, and activity are interplaying. In most of the cases, moderate activity and stickiness help the smooth transport of the probe. Because higher activity randomizes the movement and also reduces the specificity. The dynamics of the self-propelled probe in complex environments is greatly influenced by various factors such as activity, crowding density, the shape of the probe, and the confinements present in the environments. Recently, researchers have started investigating the dynamics of active probes in static environments like ordered or disordered porous media.^{23–25} This is definitely a future direction to explore, since porous media are omnipresent in biological systems, such as biological tissues and also serving as the natural habitat for many cell types. To obtain a comprehensive understanding of the underlying physics and the mechanism of the dynamics of these active probes in crowded space one has to consider the effect of all these competing factors. Altogether our model reveals some of the key features of the active probe dynamics in complex media, and further development and studies are required to attain more deeper understanding of these systems. A better understanding may help the scientists and engineers to design efficient, powerful, and better-performing artificial self-driven transport machines in crowded environments, which are considered to be next-generation drug delivery systems.¹⁶

AUTHOR INFORMATION

Corresponding Author

Rajarshi Chakrabarti – Department of Chemistry, Indian Institute of Technology Bombay, Mumbai, Maharashtra 400076, India; orcid.org/0000-0002-0785-1508; Email: rajarshi@chem.iitb.ac.in

Authors

Ligesh Theeyancheri – Department of Chemistry, Indian Institute of Technology Bombay, Mumbai, Maharashtra 400076, India; orcid.org/0000-0001-7973-4194

Rajiblochan Sahoo – Department of Chemistry, Indian Institute of Technology Bombay, Mumbai, Maharashtra 400076, India

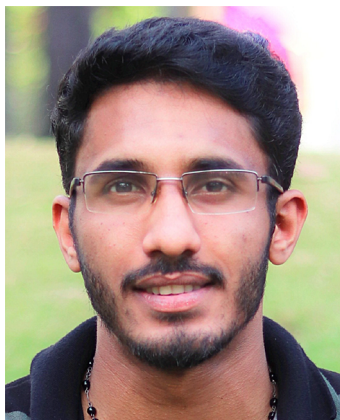
Praveen Kumar – Department of Chemistry, Indian Institute of Technology Bombay, Mumbai, Maharashtra 400076, India

Complete contact information is available at: <https://pubs.acs.org/10.1021/acsomega.2c04709>

Notes

The authors declare no competing financial interest.

Biographies



Ligesh Theyancheri is a Ph.D. student at the Department of Chemistry, Indian Institute of Technology Bombay, India, and is working with Prof. Rajarshi Chakrabarti for his doctoral thesis. He received his Master's degree from the Department of Chemistry, Central University of Rajasthan, in 2016. His current research interests are focused on understanding the dynamics of active probes in complex environments using *in silico* models.



Rajiblochan Sahoo is a Ph.D. student at the Department of Chemistry, Indian Institute of Technology, Bombay. He is working in the group of Prof. Rajarshi Chakrabarti for his doctoral thesis. He obtained his Master's degree from the Department of Chemistry, Indian Institute of Technology (Indian School of Mines), Dhanbad, in 2017. His current research focuses on the study of the dynamics of passive and active probe particles in the crowded medium using computer simulation.



Praveen Kumar is a Ph.D. student at the Department of Chemistry, Indian Institute of Technology Bombay. He is working in the group of

Prof. Rajarshi Chakrabarti for his doctoral thesis. He earned his Master's degree from the Department of Chemistry, National Institute of Technology Jalandhar (Punjab), in 2017. His current research focuses are the study of the dynamics of active and passive probe particles in a complex environment using computer simulations.



Rajarshi Chakrabarti received his Ph.D. in Theoretical Chemistry from the Indian Institute of Science, Bengaluru in 2009. His Ph.D. thesis dealt with the use of time-dependent Statistical Mechanics to investigate rate processes in the condensed phase. After two postdoctoral stints at the University of Illinois at Urbana—Champaign and the University of Stuttgart, he joined the Department of Chemistry, Indian Institute of Technology Bombay as an Assistant Professor in 2013 and rose to full Professor in 2021. His research interests are broadly in the area of Statistical Mechanics and Soft Condensed Matter. Currently he is serving as Associate Editors for Biophysics—Frontiers and the International Journal of Chemical Kinetics (Wiley).

ACKNOWLEDGMENTS

We would like to thank Raghunath Chelakkot, Subhasish Chaki, Nairhita Samanta, and Rohit Goswami for the collaboration in some of the works presented in this review. L.T. and P.K. thank UGC for the fellowships. R.S. thanks CSIR for a fellowship. R.C. acknowledges SERB for funding (Project No. MTR/2020/000230 under MATRICS scheme). The authors thank Pooja Nanavare for proofreading.

REFERENCES

- (1) Bechinger, C.; Di Leonardo, R.; Löwen, H.; Reichhardt, C.; Volpe, G.; Volpe, G. Active particles in complex and crowded environments. *Rev. Mod. Phys.* **2016**, *88*, 045006.
- (2) Tabei, S. A.; Burov, S.; Kim, H. Y.; Kuznetsov, A.; Huynh, T.; Jureller, J.; Philipson, L. H.; Dinner, A. R.; Scherer, N. F. Intracellular transport of insulin granules is a subordinated random walk. *Proc. Natl. Acad. Sci. U.S.A.* **2013**, *110*, 4911–4916.
- (3) Redner, G. S.; Hagan, M. F.; Baskaran, A. Structure and dynamics of a phase-separating active colloidal fluid. *Phys. Rev. Lett.* **2013**, *110*, 055701.
- (4) Schaller, V.; Weber, C.; Semmrich, C.; Frey, E.; Bausch, A. R. Polar patterns of driven filaments. *Nature* **2010**, *467*, 73–77.
- (5) Pecreaux, J.; Röper, J.-C.; Kruse, K.; Jülicher, F.; Hyman, A. A.; Grill, S. W.; Howard, J. Spindle oscillations during asymmetric cell division require a threshold number of active cortical force generators. *Curr. Biol.* **2006**, *16*, 2111–2122.
- (6) Gomez-Solano, J. R.; Blokhuis, A.; Bechinger, C. Dynamics of self-propelled Janus particles in viscoelastic fluids. *Phys. Rev. Lett.* **2016**, *116*, 138301.
- (7) Singh, K.; Yadav, A.; Dwivedi, P.; Mangal, R. Interaction of Active Janus Colloids with Tracers. *Langmuir* **2022**, *38*, 2686–2698.

- (8) Klett, K.; Cherstvy, A. G.; Shin, J.; Sokolov, I. M.; Metzler, R. Non-Gaussian, transiently anomalous, and ergodic self-diffusion of flexible dumbbells in crowded two-dimensional environments: Coupled translational and rotational motions. *Phys. Rev. E* **2021**, *104*, 064603.
- (9) Theeyancheri, L.; Chaki, S.; Samanta, N.; Goswami, R.; Chelakkot, R.; Chakrabarti, R. Translational and rotational dynamics of a self-propelled Janus probe in crowded environments. *Soft Matter* **2020**, *16*, 8482–8491.
- (10) Nguyen, G. P.; Wittmann, R.; Löwen, H. Active Ornstein–Uhlenbeck model for self-propelled particles with inertia. *J. Condens. Matter Phys.* **2022**, *34*, 035101.
- (11) Goswami, K.; Chakrabarti, R. Motion of an active particle with dynamical disorder. *Soft Matter* **2022**, *18*, 2332–2345.
- (12) Kumar, P.; Theeyancheri, L.; Chakrabarti, R. Chemically symmetric and asymmetric self-driven rigid dumbbells in a 2D polymer gel. *Soft Matter* **2022**, *18*, 2663–2671.
- (13) Nogueira, T.; Frota, H.; Piazza, F.; Bordin, J. R. Tracer diffusion in crowded solutions of sticky polymers. *Phys. Rev. E* **2020**, *102*, 032618.
- (14) Reserva, R. L.; Filipinas, J. L. D. C.; Jerez, M. J. Y.; Confesor, M. N. Non-equilibrium tracer dynamics in oscillating active gel. *Physica A* **2022**, *603*, 127812.
- (15) Sahoo, R.; Theeyancheri, L.; Chakrabarti, R. Transport of a self-propelled tracer through a hairy cylindrical channel: interplay of stickiness and activity. *Soft Matter* **2022**, *18*, 1310–1318.
- (16) Patra, D.; Sengupta, S.; Duan, W.; Zhang, H.; Pavlick, R.; Sen, A. Intelligent, self-powered, drug delivery systems. *Nanoscale* **2013**, *5*, 1273–1283.
- (17) Weeks, J. D.; Chandler, D.; Andersen, H. C. Role of repulsive forces in determining the equilibrium structure of simple liquids. *J. Chem. Phys.* **1971**, *54*, 5237–5247.
- (18) Plimpton, S. Fast parallel algorithms for short-range molecular dynamics. *J. Comput. Phys.* **1995**, *117*, 1–19.
- (19) Edmond, K. V.; Elsesser, M. T.; Hunter, G. L.; Pine, D. J.; Weeks, E. R. Decoupling of rotational and translational diffusion in supercooled colloidal fluids. *Proc. Natl. Acad. Sci. U.S.A.* **2012**, *109*, 17891–17896.
- (20) Zou, Q.-Z.; Li, Z.-W.; Zhu, Y.-L.; Sun, Z.-Y. Coupling and decoupling between translational and rotational dynamics in supercooled monodisperse soft Janus particles. *Soft Matter* **2019**, *15*, 3343–3352.
- (21) Ben-Isaac, E.; Fodor, É.; Visco, P.; Van Wijland, F.; Gov, N. S. Modeling the dynamics of a tracer particle in an elastic active gel. *Phys. Rev. E* **2015**, *92*, 012716.
- (22) Du, Y.; Jiang, H.; Hou, Z. Study of active Brownian particle diffusion in polymer solutions. *Soft Matter* **2019**, *15*, 2020–2031.
- (23) Kurzthaler, C.; Mandal, S.; Bhattacharjee, T.; Löwen, H.; Datta, S. S.; Stone, H. A. A geometric criterion for the optimal spreading of active polymers in porous media. *Nat. Commun.* **2021**, *12*, 7088.
- (24) Theeyancheri, L.; Chaki, S.; Bhattacharjee, T.; Chakrabarti, R. Migration of active rings in porous media. *Phys. Rev. E* **2022**, *106*, 014504.
- (25) Chopra, P.; Quint, D.; Gopinathan, A.; Liu, B. Geometric effects induce anomalous size-dependent active transport in structured environments. *Phys. Rev. Fluids* **2022**, *7*, L071101.